Energies **2015**, *8*, 8945-8961; doi:10.3390/en8088945

OPEN ACCESS

energies

ISSN 1996-1073

www.mdpi.com/journal/energies

Article

CFD Analysis of Regenerative Chambers for Energy Efficiency Improvement in Glass Production Plants

Davide Basso [1], Carlo Cravero [1], Andrea P. Reverberi [2] and Bruno Fabiano [3,*]

[1] DIME—Department of Mechanical, Energy, Logistics Engineering and Engineering Management, Polytechnic School, Genoa University, via Montallegro 1, Genoa 16145, Italy; E-Mails: davide.basso.cfd@gmail.com (D.B.); carlo.cravero@unige.it (C.C.)

[2] DCCI—Department of Chemistry and Industrial Chemistry, Genoa University, via Dodecaneso 31, Genoa 16146, Italy; E-Mail: andrea.reverberi@unige.it

[3] DICCA—Department of Civil, Chemical and Environmental Engineering, Polytechnic School, Genoa University, via Opera Pia 15, Genoa 16145, Italy

* Author to whom correspondence should be addressed; E-Mail: brown@unige.it; Tel.: +39-010-353-2585; Fax: +39-010-353-2586.

Academic Editor: Enrico Sciubba

Received: 8 May 2015 / Accepted: 17 August 2015 / Published: 24 August 2015

Abstract: The overall efficiency of a regenerative chamber for a glass furnace mainly relies on the thermo-fluid dynamics of air and waste gas alternatively flowing through stacks of refractory bricks (checkers) determining the heat recovery. A numerical approach could effectively support the design strategies in order to achieve a deeper understanding of the current technology and hopefully suggest new perspectives of improvement. A computational fluid dynamics (CFD) scheme for the regenerator is proposed, where the real geometry of the solid phase is modelled as a porous solid phase exchanging heat with the gas stream. Satisfactory data fitting proved the reliability of the present approach, whose applications are proposed in the last section of this study, to confirm how such a CFD modelling could be helpful in improving the overall energy efficiency of the regeneration chamber.

Keywords: CFD; energy efficiency; glass process plant; regenerator

1. Introduction

In the whole of the process industry, attention is focused towards prevention by inherent safer features and rethinking the processes: these trends do not hold only for safety, health, and environmental protection, but of course also for product quality, energy management, and process operability [1]. On this basis, quality standards and process efficiency must be fulfilled at the same time in glass production, despite the fact that this industrial sector is traditionally quite conservative towards innovation or experimentation. Such a skepticism could be related to the inherent difficulties in managing a process which expected lifetime spans over a period ranging from five to eight years of continuous production. As a consequence, a numerical approach can be helpful in predicting the yield of the aforementioned processes, in delivering guidelines for an environmentally sounder glass industry and in assessing the validity of innovative solutions. Furthermore, such a technique proves to be successful in matching the operating regimes of glass furnaces with those pertaining to other plant units downstream. In this context, one of the most important aspects is related to the fluid dynamics of regenerative chambers for end port furnaces. The heat recovery in regenerative chambers for glass furnaces is obtained by switching the fluid flow through assembled refractory structures called "checkers". The heat of waste gas is absorbed by the refractory bricks (hot period) and then released to the combustion air when the cycle swaps (cold period) about every 20 min.

Figure 1 schematically depicts some examples of different geometries concerning the shape of bricks and their relevant modular arrangement according to specific requirements of energy optimization and ease of disassembling during maintenance operations.

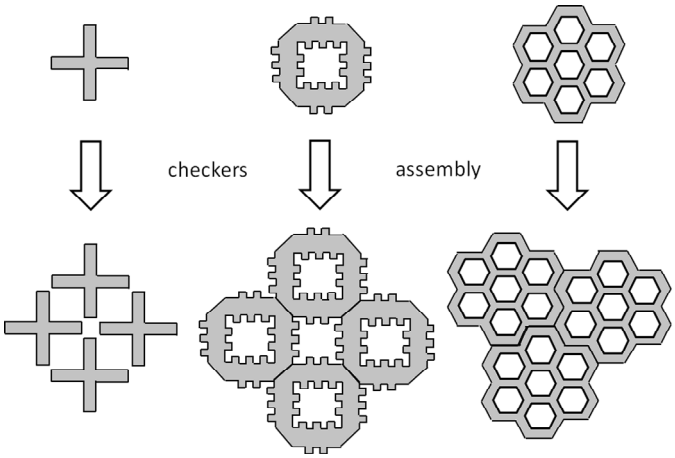

Figure 1. Examples of checker brick sections and their assemblies.

Despite few major improvements due to material technology evolution, it is widely reported that the regenerator model here considered is still the heritage of the 1850 Martin-Siemens open heart furnace, ensuring a heat recovery efficiency level of 60%–68% compared to a theoretical limit value of 75%–80%, depending on the type of fuel and process parameters [2]. Such a relatively small value can be explained remembering that the mass flow rate and specific heat transfer coefficient of air are lower than for waste gas, so that not the whole of the heat provided during the hot period can be recovered during the cold period. Likewise different high-energy consumption and high-pollution furnace processes [3], heat recovery, and energy efficiency represent research topics of major importance.

A recent approach to improve thermal efficiency of packing with a higher heat exchange rate was based on a new refractory cruciform design [2]. In an ideal case, the optimization of furnace performance would be based on adjusting operational variables, as demonstrated by the rigorous optimization of burners performed in a European oxygen-gas fired glass furnace [4]. Several theoretical studies focused on modelling the thermodynamics of a fixed bed regenerator are available in the scientific literature (e.g., [5,6]). A model for the estimation of regenerator performance under different furnace loading conditions was recently developed according to a simplified approach where the overall heat transfer coefficient is calculated for a steady state condition and corrected for cyclic operation [7]. Reboussin *et al.* [8] proposed a computational fluid dynamics (CFD)-based procedure to estimate a global thermal coefficient for the checkers with calculations for a single channel and data validation for an experimental Saint-Gobain regenerator. In their study, the disposal of refractory bricks inside the checkers is arranged to form a dense array of vertical channels. Despite the merit of this ansatz, we remark that their single-channel approach would imply an excess of computational burden if applied to a full scale geometry (as explained in the next sections), thus the aim of the present work consists of extending the fluid-dynamical analysis to the whole regenerator so that it could be a reliable tool for the designers, while maintaining a good level of accuracy. The basic idea inspiring this work relies upon extending the aforementioned modelling to the whole checkers zone, using a CFD module capable of overcoming the previously outlined drawbacks. The remainder of this paper is as follows: in Section 2, we provide a description of the plant, including some details concerning the geometry and the structure of the elements characterizing the heat exchanger. In Section 3, we outline the numerical modelling paying rigorous attention to the discretization technique and to some simplifying assumptions concerning the thermodynamics of the gas streams. In Section 4, the results concerning the temperature, pressure and velocity profiles inside the regenerator chamber are presented and two different configurations in the chamber geometry are compared in terms of efficiency optimization, utilizing as well smoke experimental data. Finally, in Section 5 we draw conclusions and outline the direction of future works.

2. Plant Layout

As depicted in Figure 2, a typical regenerative chamber for the glass industry consists of three zones: the top chamber, the bottom chamber, and the checkers in between. Each zone exerts a double role depending on the cycle: the top chamber spreads the flow from the checkers to the melting tank (cold period) and *vice versa* (hot period); analogously, the bottom chamber redistributes the flow from the waste gas port to the checkers and *vice versa*. In addition to the heat recovery, the checkers create a stack effect due to buoyancy forces. As shown by the experimental data reported in Figure 3, the top-bottom pressure profile inside the chamber during the cold period is characterized by a typical chimney behavior, with larger pressure values at the top and lower values at the bottom.

In End Port furnaces, two ports connect the melting tank at the front with two identical vertical regenerative chambers at the back (see Figure 2). The aforementioned chambers are not a part of the furnace itself, but they represent a separated structure. Under each port, three burners can be fitted as a maximum, so that the flame travels from one port toward the opposite wall of the tank making a U-turn before being discharged throughout the other port.

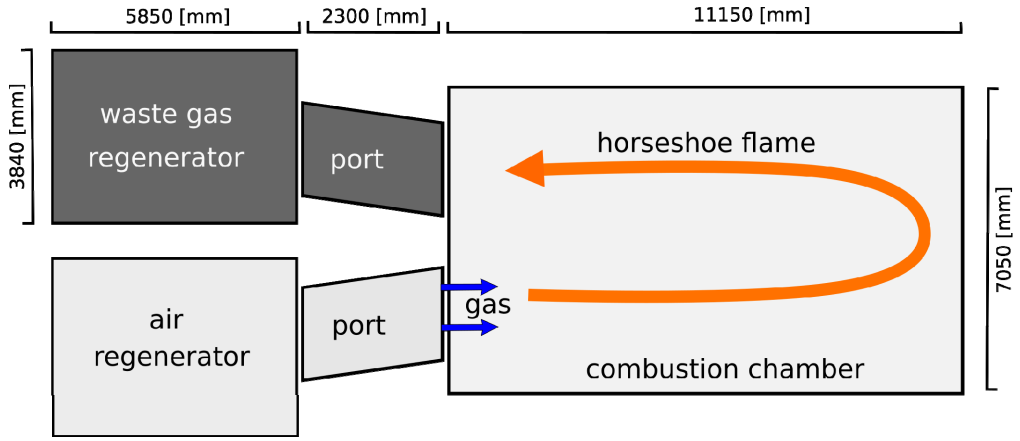

Figure 2. Plant layout of a typical End Port furnace for soda-lime glass production.

The resulting horseshoe shaped flame is one of the main advantages of this kind of furnace since, if compared with different configurations, it is characterized by a longer flame residence time ensuring a uniform and effective heat release profile.

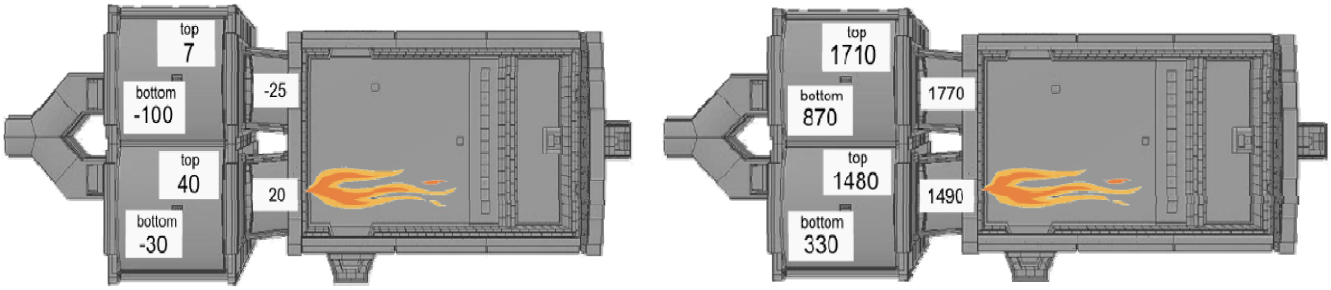

(**a**) (**b**)

Figure 3. Experimental data of a standard End Port regenerative chamber (**a**): relative pressure [Pa]; (**b**): temperature [K]).

Inside each one of the two regenerators, thousands of refractory bricks are piled up in stacks to form a thick array of vertical channels several meters tall (see Figure 4). Typically, the bricks are electrically molten refractory products based on an alumina-zirconia-silica composition (AZS) allowing high thermal and corrosion resistance in contact with aggressive environments. These technical requirements are essential for the economic sustainability and evolving constraints of the glass manufacturing process.

It is intriguing to observe that, during the phase when the checkers are heated by the gases coming from the furnace, the bricks are subject to high chemical stress owing to the compounds present in gas furnace emissions. In particular, we can name nitrogen oxides, sulfur trioxide, sulfur dioxide, and free halogens. Among the latter compounds, though being present only in traces generally not exceeding 10 parts per million (ppm), fluorine is one of the most active agents capable of triggering unexpected corrosion processes even on relatively inert materials, owing to its extreme chemical reactivity which is greater than any other electronegative element.

In order to realize the heat recovery, the flow path is switched from one chamber to another at constant time intervals (approximately 15–20 min).

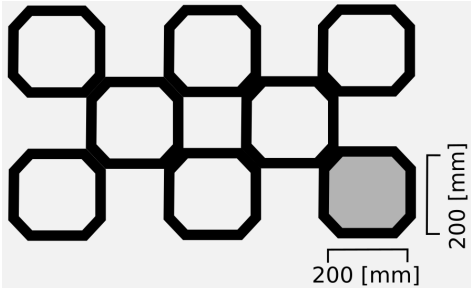

Figure 4. Schematic view of the checker bricks disposal inside the regenerator considered in the present study.

The flow velocity can vary up to an order of magnitude inside the chamber: in the given plant for example, during the cold period, air is blown into the Bottom Chamber through the port at about 1.2 $m \cdot s^{-1}$ while, at the Top Chamber, it accelerates in the port up to 12 $m \cdot s^{-1}$ before entering the combustion chamber. Similarly, for the hot period, we have 13 $m \cdot s^{-1}$ at the port and 2.5 $m \cdot s^{-1}$ in the duct (since the mass flow rate and temperatures of waste gases are higher than for air). The Reynolds number values for air and waste gas evaluated at the inlet condition based on the hydraulic diameter are about 1.4×10^5 and 7.5×10^4 respectively.

As previously stated, buoyancy is an important aspect inside the regenerative chambers and its role inside the checkers was assessed considering the Richardson number:

$$Ri = \frac{g \Delta \rho L}{\rho_a U^2} \tag{1}$$

evaluated according to the following data: density gradient between top and bottom chamber, $\Delta\rho = 0.9$ $kg \cdot m^{-3}$; characteristic vertical length $L = 0.15$ m corresponding to the hydraulic diameter of one channel (see Figure 4); average reference density $\rho_a = 0.65$ $kg \cdot m^{-3}$; reference velocity $U = 1$ $m \cdot s^{-1}$.

With the aforementioned data, we obtained $Ri \cong 2.04$, a value consistent with the actual role of the buoyancy forces.

3. Theoretical Modelling

The overview of a typical End Port furnace shown in Figure 1 illustrates that, despite the geometry of the chamber being rather simple, at the same time the piles of checker bricks create a complex and very large structure. The cross-section of one brick is about 200×200 mm^2 and it would require a mesh size of less than 20 mm to fill a fluid domain of nearly 120–150 m^3. Clearly, this requirement implies a heavy burden in terms of memory and computational time and it is indeed far beyond the purpose of this work. A well-established technique for similar problems [9] relies upon adopting a porous model set-up to conveniently capture the physics inside the checkers, instead of describing the real geometry.

The pressure values presented in Figure 3 are time averaged over one-minute sampling, performed by a portable analyzer. The estimated error is about ±1 Pa.

Collection of reliable temperature data is more critical. The furnace is equipped with control structure-embedded thermocouples located inside the plant but their measurements are not entirely

reliable due to overestimation, mainly in the presence of radiation. The estimated temperature error is in the range of 20–30 degrees.

3.1. Geometry and Numerical Details

The discretization of the embedding space often represents a crucial aspect common to other modelling problems concerning heat [10] and mass transfer/diffusion [11] in many disciplines pertaining to both technical and scientific literature. Following the chamber scheme of Figure 5, four different domains were meshed separately and then joined together through interfaces. The commercial code ICEM (Integrated Computer Engineering and Manufacturing)-CFD was used and its blocking technique applied to each domain to obtain high quality fully hexahedral meshes in the distinct regions of the control domain, according to a simulation approach successfully applied in modelling coke oven chambers used in coal dry distillation plants [12]. In this way, as shown in Figure 6, we focused on the bottom chamber meshing by properly taking into account its structurally complicated geometry with a spatial resolution of about 20 mm. The final grid comprised 4.0×10^6 cells with a minimum orthogonality value of 0.63 and a maximum aspect ratio of 4. This grid allowed satisfactory results to be obtained when compared with the experimental data presented in Figure 3. An alternative coarser mesh also gave acceptable results but with a weaker convergence level; the 4M cells mesh guaranteed a tighter convergence of the normalized residuals for continuity (around 10^{-4}) and momentum equation (around 10^{-5}).

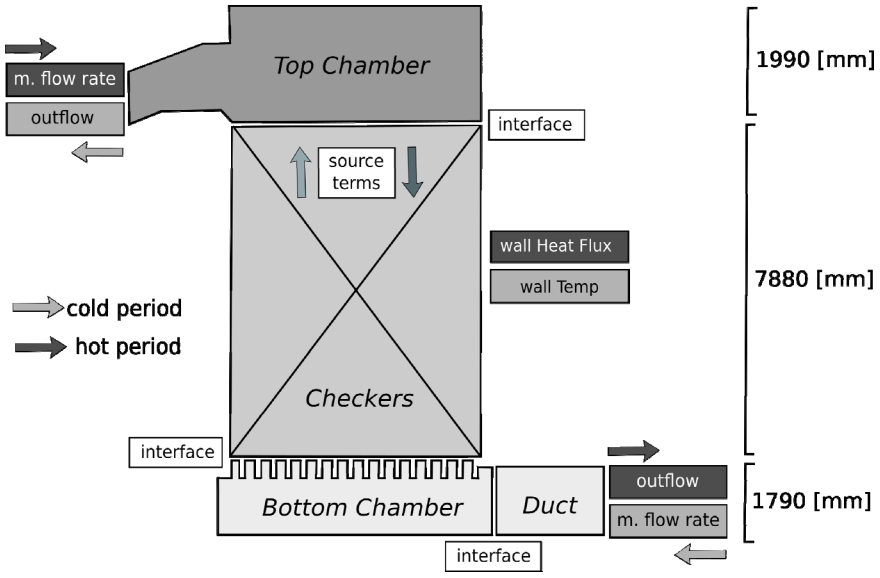

Figure 5. Schematic view of the regenerator structure with the relevant boundary conditions.

Some of the material properties and environmental conditions were simplified to avoid additional algorithmic complications: continuity, momentum, turbulence, and energy balances were modelled according to standard and well established CFD procedures [13]. More specifically, SIMPLE steady-state algorithm (Semi-Implicit Method for Pressure Linked Equations) was used for the calculations, with second order accurate discretization schemes for all equations. *K*-ε standard scheme was used for turbulence modelling and since different velocity scales inside the domain lead to $y+$ values ranging from 60 to10, adjusted scalable wall-functions were adopted.

The data reported in the aforementioned Figure 3 suggest two preliminary considerations: first, the thermal gradients are very large, as the temperature dependence of gas properties cannot be neglected; second, the pressure distribution of the air chamber is typical of a buoyancy driven flow (stack effect) with the higher values downstream of the checkers and the lower values upstream. Hence, in order to simulate appropriately the system under conditions close to reality, it is mandatory to determine the role of temperature on the fluid and the actual resulting buoyancy variation.

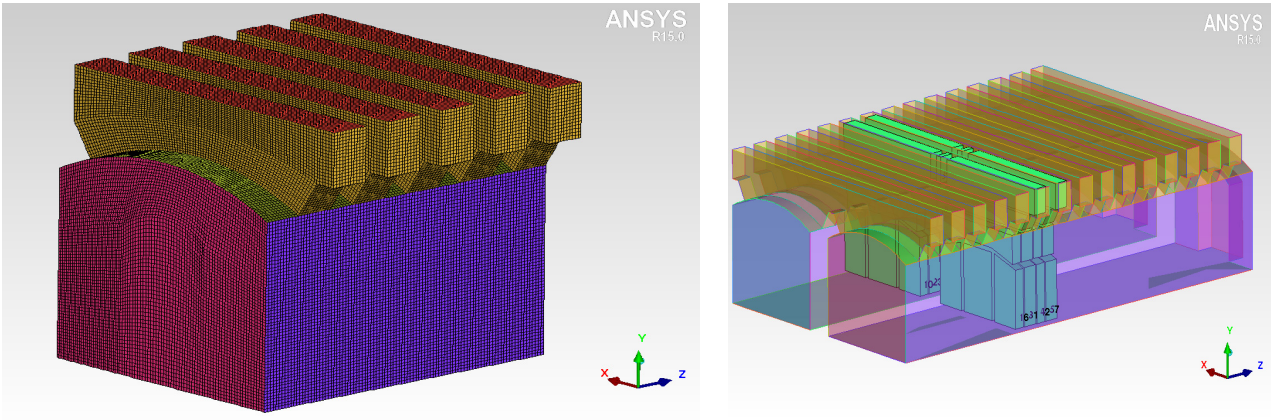

(**a**) (**b**)

Figure 6. Blocking approach (**a**) and resulting mesh (**b**) for the bottom chamber.

3.2. Governing Equations

Both waste gases and air were considered as a mixture of different gases, whose thermo-physical properties were modelled as follows [6,8,14]:

- The viscosity μ is determined according to the Sutherland formula, which proved to be satisfactory for several gases in a wide range of temperature *T*. For each gas, a specific value of the parameter *S*, the Sutherland constant, is put into the following expression:

$$\frac{\mu}{\mu'} = \frac{T' + S}{T + S}\left(\frac{T}{T'}\right)^{3/2} \tag{2}$$

where $T' = 273$ K and $\mu' = \mu(T')$ are reference values. This expression tends to increasingly underestimate the viscosity of the fluid above 1000 K. Nevertheless, the error at 1773 K (corresponding to highest temperature value in the calculations performed for the hot period) is around 5%, namely an acceptable value given the purpose of this study.

- The equation of state for ideal gases supplies the simplest link between the density, ρ, the average molecular weight, *M,* and the other thermodynamic variables of the process as follows:

$$\rho = \frac{pM}{RT} \tag{3}$$

- The specific heat at constant pressure c_p can be conveniently described by a fourth-order polynomial expression as from the NIST Database [15], namely:

$$\frac{c_p}{R} = a_1 + a_2 T + a_3 T^2 + a_4 T^3 + a_5 T^4 \tag{4}$$

where R is the universal gas constant and the values of coefficients a_i are those pertaining to air. Despite the seemingly simple approximation, this choice proved to be satisfactory in data validation, as is shown in the following.

- The thermal conductivity λ is evaluated according to the Eucken Modified approximation based on the kinetic theory of gases, as follows:

$$\frac{\lambda}{\rho c_v} = 1.32 + \frac{1.77}{(c_p / R - 1)} \tag{5}$$

The introduction of mass balance equations for each chemical species in the gas streams can be useful to make a comparison between the numerical results and the experimental chemical analyses. Since no detailed experimental data can be obtained on the velocity fields inside the chambers, the concentrations of the chemical species represent a useful marker in order to obtain further information on the flow under different operating conditions, as discussed in the applications.

Inside the checkers, three major physical phenomena can be recognized: heat exchanges between the fluid and the refractories, temperature induced buoyancy forces, and head losses caused by the obstruction of the checkers to the flow. As far as heat exchange inside the porous domain is concerned, two possible approaches exist. In the former, a thermal equilibrium between the solid and the fluid phase is assumed, while in the latter the two phases are treated separately. Despite the latter hypothesis being often adopted in regenerator modelling, it poses problems of stability and convergence that are currently beyond the purpose of the present study. Namely, the non-equilibrium approach requires the knowledge of global thermal coefficients to model the solid-fluid heat exchange. A correct estimation of such coefficients during both periods of the regenerator would imply additional information about many physical aspects concerning natural/mixed convection and radiation. On the other hand, when temperature data are available inside the regenerator (which is very often the case), the equilibrium approach is nevertheless appropriate and less demanding.

The conservation equation, in divergence conservative form, for internal energy h can be expressed as follows [16]:

$$\frac{\partial(\rho h)}{\partial t} + \operatorname{div}(\rho h \boldsymbol{u}) = -p \operatorname{div} \boldsymbol{u} + \operatorname{div}(\lambda \operatorname{grad} T) + S_i \tag{6}$$

Under equilibrium hypothesis, we assume that the temperature gradients occur almost entirely inside the checkers and a volumetric source/sink term S_i, whose magnitude is estimated by the temperature experimental data in order to take into account the inter-phase heat exchange, is present at the right hand side of the previous equation. S_i can be evaluated by means of integration of the specific heat at constant pressure for the i-th fluid between the measured temperature values at upstream (T_1) and downstream (T_2) side of the checkers; namely:

$$S_i = \frac{W_i}{V} \int_{T_1}^{T_2} c_{p_i}(T)\, dT \tag{7}$$

where F_i is the mass flow rate of the i-th fluid and V is the total apparent volume of the porous medium.

On this basis, heat flux between gas and solid (checkers) is modelled using the aforementioned source term as a specific heat flux; we estimated it using reference inlet/outlet temperatures and mass

flow rates from experimental data measured *ad-hoc* or acquired from the process monitoring system, under steady-state operation.

The momentum balance equation can be written as:

$$\frac{\partial(\rho \boldsymbol{u})}{\partial t} + \operatorname{div}(\rho \boldsymbol{u}\boldsymbol{u}) = -\operatorname{grad} p + \operatorname{div} \boldsymbol{\tau} + (\rho - \rho_0)\boldsymbol{g} + \boldsymbol{S}_p \tag{8}$$

where τ is the shear stress tensor. The gravitational term included corresponds to the so-called "fully buoyant" approach since the temperature gradients are large across the domain and Boussinesque-like approximations of buoyancy do not seem to be suitable for this case study.

The resistance exerted by the porous medium on the gas stream was also modelled with the addition of a volumetric source term $\boldsymbol{S_p}$ to the momentum equation. This term is the sum of viscous and inertial contributions which, in the most general case, can be different for the three directions in space. On the other hand, the gas flow along the checkers has a preferential vertical direction, as the piles of bricks form a structure very similar to a tube bundle where the cross-flow between neighboring tubes is strongly inhibited (if not completely blocked). Thus, the corresponding porous model must preserve a high anisotropy and its resistance coefficients were calculated only for the vertical direction. For the remaining directions, resistance coefficients values up to three orders of magnitude higher were chosen in order to ensure the onset of a vertical velocity field. Finally, the momentum source/sink term for the *i*-th cartesian direction can be written as:

$$S_{p,i} = -\left(\frac{\mu}{\alpha_i} u_i + C_i \frac{\rho}{2} |u| u_i \right) \tag{9}$$

The first term on the right-hand side of Equation (9) is related to viscous losses (Darcy law), while the second one accounts for inertial losses.

For the calculation of vertical porous permeability α_y and inertial resistance factor C_y, a 1.5 m length "checker tube" was considered (as shown in Figure 7) and several calculations at different bulk velocities were performed, so as to obtain the resulting pressure gradient. These data, plotted on a pressure-velocity plane, can be fitted with a quadratic polynomial form as follows:

$$S_{p,i} = -\frac{\Delta p}{\delta} = \left(k_1 u_{bulk}^2 + k_2 u_{bulk} \right) \tag{10}$$

where δ is the thickness of the porous medium, Δp is the corresponding head loss, and u_{bulk} is the average fluid velocity. The coefficients k_1, k_2, α_i, and C_i are estimated by comparison of Equations (9) and (10) and they are given as input to the software here adopted.

As depicted in Figure 8, we considered both top and bottom thermal conditions of the checkers in order to account for the frictional losses dependence upon the constantly varying fluid properties along the checkers. The porous resistance coefficients inside the model are supposed to vary linearly between top and bottom. The proposed approach was applied in the simulation of both air flow and waste gas cycles, adopting the domain boundary conditions summarized in the already mentioned Figure 5. Since mass flows are known data for a given chamber, they can be easily enforced as inlet boundary conditions; if the calculation involves mixing fluids (*i.e.*, waste gas recirculation application, as will be briefly discussed in the next section) the molar concentration of each compound must be specified as well. At the outlet of the domain, the Neumann "outflow" boundary condition ensures the best

convergence of the residuals; moreover, the Inlet-Outlet pressure gradient across the domain is not imposed but it offers a first test for the reliability of the approach. Thermal boundary conditions at the wall are implemented differently depending on the evolving fluid: during the air period, the wall temperatures are applied to the domain boundaries while a negative (cooling) heat flux is imposed for the waste gas period. Interfaces at the porous domain boundaries do not require particular conditions but they need interpolation between non-conformal surface meshes. The error introduced at the interfaces is limited despite local grid dimensions having been kept equal on both sides of the embedding space. As far as the single tube calculations are concerned (see Figure 7), a similar set of boundary conditions was applied with the exception of a symmetry condition at the lateral openings of the bricks. A hole is present on each side of a single brick both to reduce the weight of the brick and to avoid preferential paths of the fluid in case of clogged tubes.

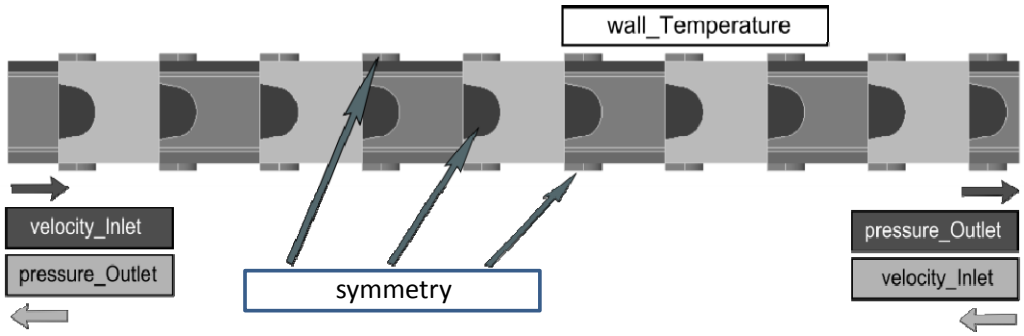

Figure 7. Computational domain and boundary conditions for the tube sample.

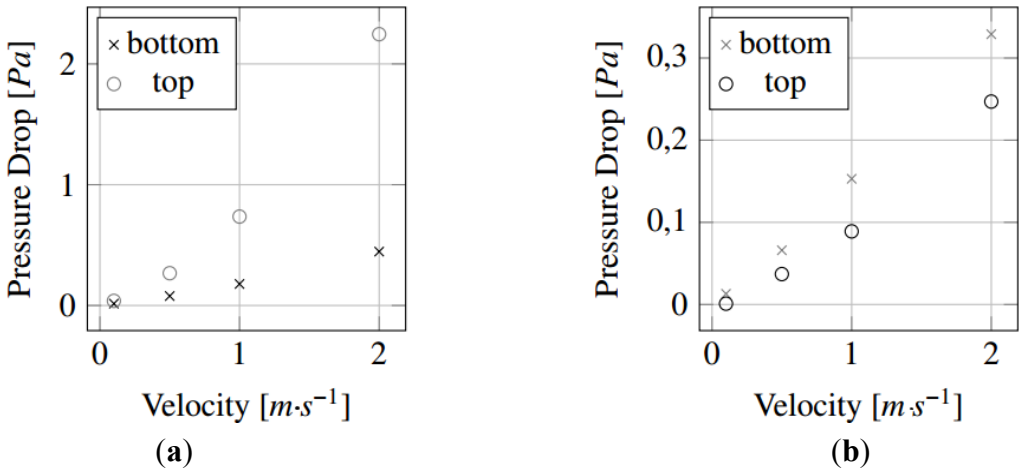

Figure 8. Different head loss profiles *versus* velocity, for cold (**a**) and hot period (**b**) of the regenerator. Top and bottom refer to different temperature conditions of fluids at the two sides of the checkers.

With the only exception of the bricks close to the lateral walls of the checkers zone, each tube is linked with four adjacent tubes: a symmetry condition is more suitable for the openings of the bricks in order to account for this recursive pattern.

4. Results and Discussion

The calculations were performed by the commercial CFD code ANSYS-Fluent® (ANSYS Inc., Canonsburg, PA, USA) over the whole chamber domain, for both air and waste gas cycles. We developed the regenerator model of ANSYS-Fluent® as it had been successfully adopted to evaluate the performance of new cruciform refractory solution in a glass furnace, at an affordable computational cost [2]. Several simulation runs were firstly performed to analyze the variations of temperature fields throughout the different process phases. As an example, Figure 9 shows the temperature profiles for both air and exhaust gases at a middle transversal section of the regenerative chamber. The effect of thermal energy transfer is clearly visible and the different flow distribution due to flow direction (bottom-top for air and top-bottom for exhausts) can be detected in the contour pattern.

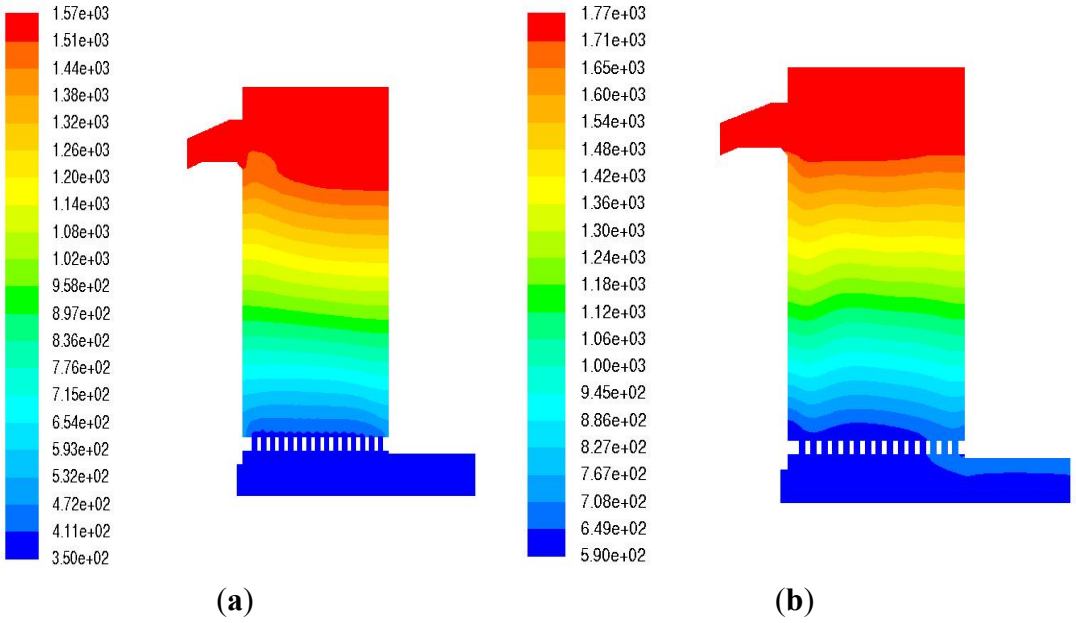

Figure 9. Temperature [K] distribution during air flow (**a**) and exhaust gases flow (**b**).

Figure 10 shows the flow pattern of air and waste gas for a typical chamber configuration and it clearly explains how the flow is strongly forced in the vertical direction inside the checkers. The pressure streamlines show that there is a gradient of about 120 Pa for waste gases and 60 Pa for air between top and bottom chambers, a result which is in fairly good agreement with the experimental data of 107 Pa and 70 Pa respectively. Looking at the air cycle, it appears that the flow is quite smooth along the chamber and that the flow recirculation is induced by the solid structure. In the waste gas cycle, the streamlines from the port to the checkers are quite complicated with a strong recirculation pattern that would endanger the flow uniformity inside the chamber. This trend represents a key aspect for both the structural integrity and the thermal efficiency of the regenerative chamber. The present CFD model can effectively explain the effect of the chamber aspect ratio on the flow homogeneity at the chamber top and on the overall thermal efficiency of the system. In Figure 11, the results of such an analysis are shown: the vertical component w of the velocity vector is contoured on the regenerator top plane and the values of the relative standard deviation σ_w for the w-velocity distribution on the same control plane are given. Longer chambers avoid impingement of the flow into the opposite wall

(as visualized in the square chamber on the left-hand side of the above Figure 11) and enhance the actual quality of the flow feeding the checkers.

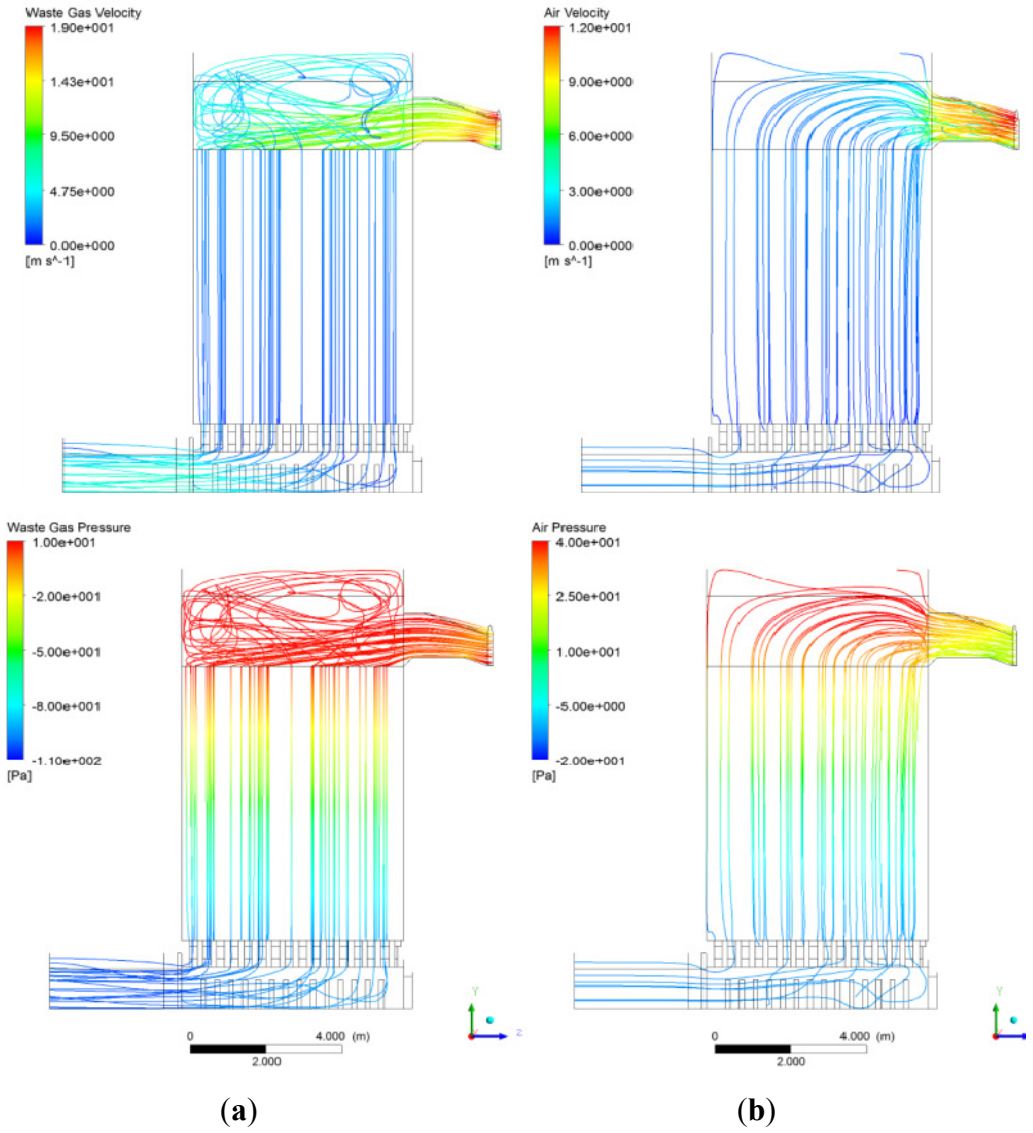

Figure 10. Pressure and velocity streamlines for waste gas (**a**) and air flow (**b**) cycles.

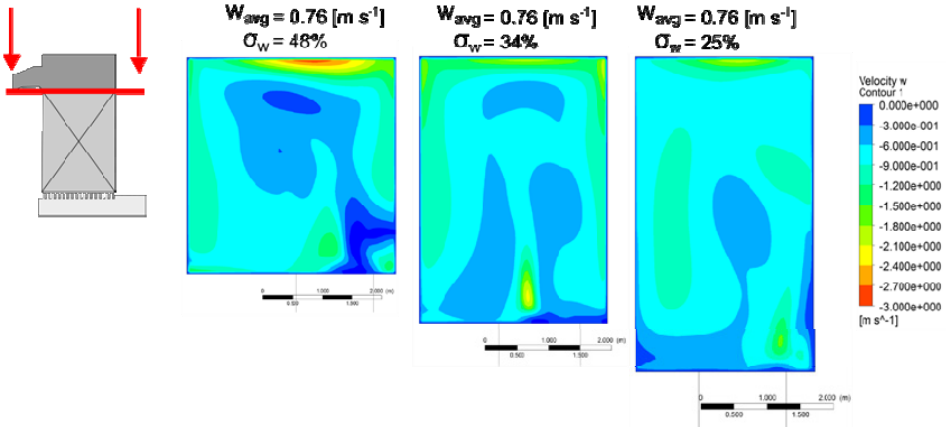

Figure 11. Homogeneity analysis of waste gas flow for different aspect ratios of the chamber. W_{avg} [m·s^{-1}] is the average vertical velocity, while σ_w is its relative standard deviation.

A further practical application of the CFD model consists of redesigning the ducts for a chamber where the uneven discharge of waste gas mass flow could reduce the overall regenerator performances, as clearly visible in Figure 12.

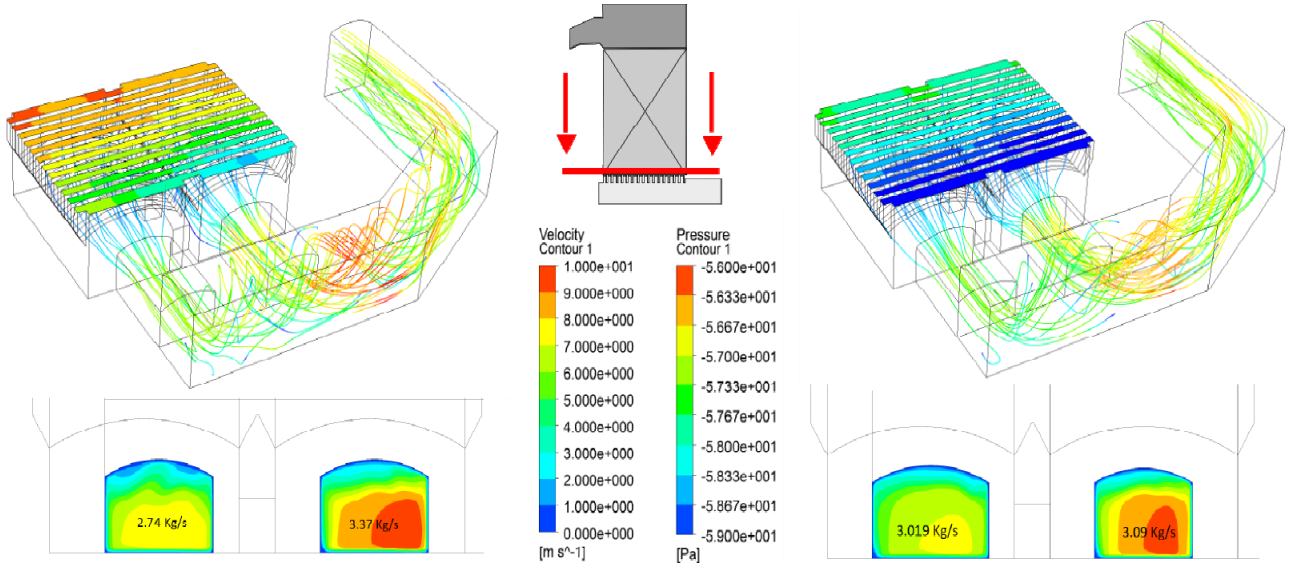

Figure 12. Duct original design and plant modification according to the proposed computational fluid dynamics (CFD) modelling.

This knowledge can help identifying areas that need special design or control to ensure safe and reliable plant operation. The original design (Figure 12, left snapshot) consisted of two identical ducts connecting the bottom chamber with the main duct. A series of CFD simulations allowed us a quantitative verification of an imbalance in mass flow rates connected to the designed configuration (2.74 kg·s^{-1} in the left duct compared to 3.37 kg·s^{-1} in the right duct). The sharp non uniformity in the exhaust hot gases distribution and consequent high temperature result in a reduced thermal efficiency of the regenerator. After a proper redesign and verification procedure, based on the CFD model, the problem was correctly overcome (Figure 12, right snapshot). A different cross section for the two ducts was introduced according to the 3D flow structure simulated by the numerical approach and almost equal mass flow rates were obtained for the two exit ducts (3.019 kg·s^{-1} in the left duct and 3.09 kg·s^{-1} in the right duct). Additionally, as clearly evidenced in the same Figure 12, the modified plant configuration is characterized by a more uniform pressure distribution at the control plane (regenerative chamber bottom section), with positive effects for both flow and thermal uniformities and connected reduced structural stress.

A further noteworthy application and a strong opportunity for CFD model validation is connected to the development of a waste gas recirculation technique. Namely, a certain percentage of waste gases is injected into the combustion air in order to lower the oxygen concentration obtaining a milder combustion with a reduction in nitrogen oxides production, consistent with an inherent safety approach through the guideword "attenuation". The only modification to the model described so far, is the distribution of gas composition at the bottom chamber inlet to identify the clean air and the (recirculated) waste gas mass flow inlet. The CFD analysis gives the flow path of the waste gases through the regenerator from the bottom chamber up to the port in the upper part. The above

recirculation strategy was investigated and designed for an existing glass production plant according to the CFD simulations here outlined. The optimal solution developed according to the simulation campaign was adopted in the final detailed design of the plant. After the installation of the gas recirculation system, several experimental series were performed on site and the measured quantities were used to validate the flow pattern predicted by simulation runs.

The concentrations of chemical compounds were measured by means of an analyzer (Testo S.p.A., Milan, Italy) equipped with suitable electrochemical cells for the quantitative analysis of O_2, CO, NO_x, and SO_x at high sampling rates (accuracy ± 0.8% for oxygen, 5% for other compounds; resolution 0.1% *v*/*v*). The smoke is passed into a properly designed sequential system, already tested at similar severe operating conditions [17], allowing after sampling, cooling, dehumidification, and retention of particulate matter, also useful in view of the analysis of further smoke compounds. It is worth recalling that these kind of experimental series carried out within an industrial furnace plant suffer from severe limitations of the sampling procedure, mainly due to the limited access to the system and to extreme local environmental conditions. As a consequence, a limited number of measuring positions in the top section plane were considered and the control plane was divided into nine cells having the measuring point as centroid. Three measurements were considered for the port section and classified as bottom (B), middle (M) and top (T) according to the vertical sampling probe positioning. The measured concentration values were assumed as being representative of the corresponding cell of the domain. Analytical accuracy and precision were assessed by performing replicate measurements (n = 5), with calculated experimental error lower than 5%. The CFD simulation data were post-processed in order to compare them with the above experimental results and averages of local mesh values were obtained at the nine control cells. In Figure 13, a sketch of the chamber is depicted: the left snapshot refers to the top section with nine control cells, while the right one pertains to the middle cross section with three control points. Table 1 shows the resulting comparison between the actual experimental values of oxygen and carbon dioxide concentration and those resulting by CFD calculations under realistic operating conditions.

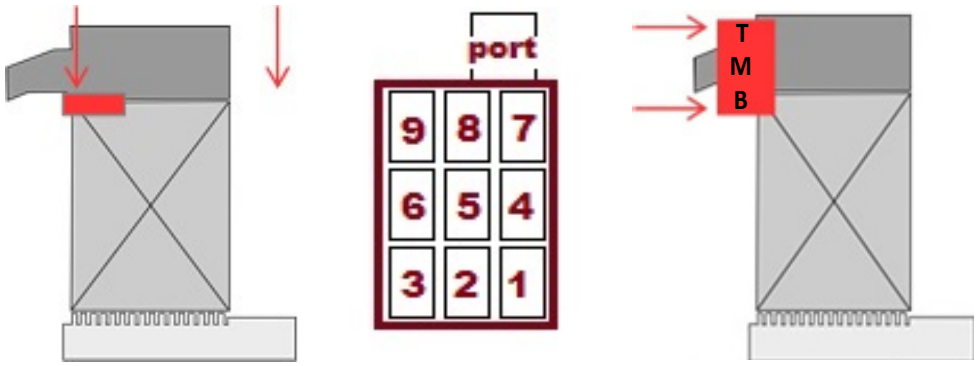

Figure 13. Schematic representation of the chamber with experimental test sections. (**a**) = top section of the checker zone where the nine control cells are put in evidence; (**b**) = cross section of the port where the measuring points defined as bottom (B), middle (M) and top (T) are localized).

Table 1. Experimental and calculated concentration (*v*/*v*) at the reference points.

Concentration	Point											
	1	**2**	**3**	**4**	**5**	**6**	**7**	**8**	**9**	**B**	**M**	**T**
$O_{2,exp}$	20.6	20.6	20.7	20.7	20.5	20.3	18.2	18.7	20	18.1	19.6	20.4
$O_{2,calc}$	20.9	20.9	20.9	20.2	20.4	20.3	17.7	18.1	17.9	17.9	19.9	20.9
$CO_{2,exp}$	0.2	0.1	0.1	0.2	0.3	0.4	2.2	1.8	2.4	2.3	1.0	0.3
$CO_{2,calc}$	0.01	0.04	0.03	0.5	0.4	0.4	2.2	1.8	2.02	2.3	0.8	0.04

The agreement between the experimental data and the numerical calculations observed on the top section for air and exhaust gases entering the chamber at the bottom plane is fairly good. This result can be interpreted as a satisfying validation of the present CFD model for the regeneration chamber under investigation. The validation results suggest that this approach can be applied in chamber simulation to obtain adjustment, control models, and hopefully design optimization, at least as a first screening tool, given the simplifying assumptions on which it relies.

5. Conclusions

The developed CFD model for regenerative chambers provided good performance in terms of flexibility, accuracy, and reliability of quantitative results. As far as energy efficiency is concerned, the computational approach could be helpful in future plant design. The porous domain assumption is realistic and the handling of heat recovery through addition of source terms to the energy equation simplifies the problem setting. Nevertheless, the major drawback of this approach is the need, *a priori*, of experimental reference temperature data. A further step in the refined model development would be the introduction of a non-equilibrium thermal model inside the porous domain. Following this refinement, the fluid and the solid phases will be handled separately by the solver and once the heat transfer mode has been properly defined, the model will be capable of giving reliable results for advanced regenerative chamber design, without the need of time consuming extensive temperature data for calibration.

Acknowledgments

This model and CFD applications to glass industry in general are currently under development within the Primeglass European Project (LIFE12 ENV/IT/001020) framework coordinated by Stara Glass S.r.l. (Genova, Italy) in partnership with University of Genova and Stazione Sperimentale del Vetro (Venezia, Italy). Experimental data were kindly provided by Stara Glass S.r.l. and Stazione Sperimentale del Vetro. For the support throughout the development of the model, their R&D department must be also acknowledged.

Author Contributions

Davide Basso, Carlo Cravero, Andrea P. Reverberi and Bruno Fabiano equally contributed to the different activities related to this scientific paper, from idea development to manuscript revision. All authors have given approval to the final version of the paper.

Conflicts of Interest

The authors declare no conflict of interest.

Nomenclature

a_i (i = 1–5)	Coefficients in the polynomial expression of the specific heat (Equation (4))
C_i	Inertial resistance factor along the i-th direction
c_p	Specific heat at constant pressure
c_v	Specific heat at constant volume
F_i	Mass flow rate of the i-th fluid
$\boldsymbol{g}$	Gravity acceleration
h	Enthalpy
k_1, k_2	Constant coefficients in Equation (10)
L	Characteristic length
M	Average molecular weight
p	Pressure
R	Universal gas constant
S	Sutherland constant in the expression of gas viscosity (Equation (2))
S_i	Source term of heat exchange between gas stream and porous solid in Equation (6)
$\boldsymbol{S_p}$	Source term in momentum balance equation
T	Temperature
T'	Temperature reference value
t	Time
U	Average gas velocity
$\boldsymbol{u}$	Velocity vector
V	Total apparent volume of the porous medium
W_{avg}	Average vertical velocity
α_i	Porous permeability along the i-th direction
δ	Thickness of the porous medium
σ_w	Relative standard deviation of vertical velocity
μ	Dynamic viscosity
λ	Thermal conductivity
ρ	Density
ρ_a	Average reference density
$\boldsymbol{\tau}$	Shear stress tensor

References

1. De Rademaeker, E.; Suter, G.; Pasman, H.J.; Fabiano, B. A review of the past, present and future of the European loss prevention and safety promotion in the process industries. *Process Saf. Environ. Prot.* **2014**, *92*, 280–291.
2. Le Chevalier, D.; Cabodi, I.; Citti, O.; Gaubil, M.; Poiret, J. New cruciform solutions to upgrade your regenerator. In *Ceramic Engineering and Science Proceedings*; Drummond, C.H., III, Ed.; John Wiley & Sons: Hoboken, NJ, USA, 2012; Volume 33, pp. 91–104.
3. Wang, Y.; Chen, H.; Chen, Z.; Ma, H.; Zhao, Q. Slagging and fouling characteristics of HRSG for ferrosilicon electric furnaces. *Energies* **2015**, *8*, 1101–1113.

4. Van Kersbergen, M.; Beerkens, R.; Sarmiento-Darkin, W.; Kobayashi, H. Optimization of burners in oxygen-gas fired glass furnace. In *Ceramic Engineering and Science Proceedings*; Drummond, C.H., III, Ed.; John Wiley & Sons: Hoboken, NJ, USA, 2012; Volume 33, pp. 3–14.
5. Koshelnik, A.V. Modelling operation of system of recuperative heat exchangers for aero engine with combined use of porosity model and thermo-mechanical model. *Glass Ceram.* **2008**, *65*, 301–304.
6. Zarrinehkafsh, M.T.; Sadrameli, S.M. Simulation of fixed bed regenerative heat exchangers for flue gas heat recovery. *Appl. Therm. Eng.* **2004**, *24*, 373–382.
7. Sardeshpande, V.; Anthony, R.; Gaitonde, U.N.; Banerjee, R. Performance analysis for glass furnace regenerator. *Appl. Energy* **2011**, *88*, 4451–4458.
8. Reboussin, Y.; Fourmigu, J.F.; Marty, P.; Citti, O. A numerical approach for the study of glass furnace regenerators. *Appl. Therm. Eng.* **2005**, *25*, 2299–2320.
9. Yakinthos, K.; Missirlis, D.; Sideridis, A.; Vlahostergios, Z.; Seite, O.; Goulas, A. Modelling operation of system of recuperative heat exchangers for aero engine with combined use of porosity model and thermo-mechanical model. *Eng. Appl. Comput. Fluid Mech.* **2012**, *6*, 608–621.
10. Solisio, C.; Reverberi, A.P.; Del Borghi, A.; Dovì, V.G. Inverse estimation of temperature profiles in landfills using heat recovery fluids measurements. *J. Appl. Math.* **2012**, *2012*, doi:10.1155/2012/747410.
11. Reverberi, A.P.; Maga, L.; Cerrato, C.; Fabiano, B. Membrane processes for water recovery and decontamination. *Curr. Opin. Chem. Eng*. **2014**, *6*, 75–82.
12. Palazzi, E.; Currò, F.; Fabiano, B. Accidental continuous releases from coal processing in semi-confined environment. *Energies* **2013**, *6*, 5003–5022.
13. Gómez, M.A.; Álvarez Feijoo, M.A.; Comesaña, R.; Eguía, P.; Míguez, J.L.; Porteiro, J. CFD simulation of a concrete cubicle to analyze the thermal effect of phase change materials in buildings. *Energies* **2012**, *5*, 2093–2111.
14. Reverberi, A.P.; Fabiano, B.; Dovì, V.G. Use of inverse modelling techniques for the estimation of heat transfer coefficients to fluids in cylindrical conduits. *Int. Commun. Heat Mass Transfer* **2013**, *42*, 25–31.
15. National Institute of Standards and Technology (NIST). Standard Reference Database Number 69. Available online: http://webbook.nist.gov/chemistry/ (accessed on 27 April 2015).
16. Anderson, J.D. *Computational Fluid Dynamics—The Basics with Applications*; McGraw Hill: New York, NY, USA, 1995.
17. Vianello, C.; Fabiano, B.; Palazzi, E.; Maschio, G. Experimental study on thermal and toxic hazards connected to fire scenarios in road tunnels. *J. Loss Prev. Process Ind*. **2012**, *25*, 718–729.